Asian Journal of Chemistry; Vol. 34, No. 7 (2022), 1869-1874

ASIAN JOURNAL OF CHEMISTRY

https://doi.org/10.14233/ajchem.2022.23766

Structural and Optical Properties of Dy^{3+} Doped with an Eulytite Type $NaBaBi_2(PO_4)_3$ Phosphor for White Light Emitting Diodes

K. INDUMATHI[1], S. TAMILSELVAN[1,*], A. DUKE JOHN DAVID[2], G. SHAKIL MUHAMMED[3] and G. ANNADURAI[4]

[1]Department of Physics, Arignar Anna Government Arts College, Cheyyar-604407, India
[2]Department of Physics, Voorhees College, Vellore-632001, India
[3]Department of Physics, Islamiah College, Vaniyambadi-635752, India
[4]College of Physics and Optoelectronics, Taiyuan University of Technology, Taiyuan 030024, P.R. China

*Corresponding author: E-mail: stsresearch1977@gmail.com

Received: 6 February 2022; *Accepted*: 28 May 2022; *Published online*: 15 June 2022; AJC-20868

A series of $NaBaBi_{(2-x)}(PO_4)_3$:xDy^{3+} eulytite type phosphors with varying doping concentrations were synthesized using a conventional solid-state reaction. The crystalline nature and phase formation of the phosphor were confirmed by the PXRD technique. FESEM was used to examine the surface morphology. UV-DRS measurements were used to quantify the band gap of the host and Dy^{3+} ion doped phosphors. The phosphors' photoluminescence properties were thoroughly investigated. According to the excitation spectra, these phosphors show a strong absorption band in the near-ultraviolet (NUV) region, extending from 250 to 450 nm. Under the excitation of 352 nm, the peaks of the emission spectra of Dy^{3+} ions are located at 485 nm (blue), 575 nm (yellow) and 666 nm (red), corresponding to the magnetic dipole $^4F_{9/2}\rightarrow{}^6H_{15/2}$ transition, the electric dipole $^4F_{9/2}\rightarrow{}^6H_{13/2}$ transition and the $^4F_{9/2}\rightarrow{}^6H_{11/2}$ transition. The optimal concentration of Dy^{3+} doped phosphor is $x = 0.075$ and the major concentration quenching mechanism is accomplished by energy transfer between the nearest-neighbour ions. The critical transfer distance (R_c) is estimated to be about 19.01. The Commission International deI'Eclairage (CIE) of $NaBaBi_{1.925}(PO_4)_3$:$0.075Dy^{3+}$ phosphor was calculated to be ($x = 0.341$ and $y = 0.374$), which was very close to the "ideal white" ($x = 0.33$, $y = 0.33$). Present findings suggest that the phosphor might be a viable option for producing a white-light-emitting phosphor under NUV activation.

Keywords: Phosphor, Eulytite, Chromaticity coordinates, Activators, Phase formation.

INTRODUCTION

In present solid state lighting research domain, the need for phosphor converted white light emitting diodes (WLEDs) has driven researchers to design revolutionary phosphors with adequate host matrix doped with suitable activators [1]. Light-emitting diodes (LEDs) have received significant attention as illuminating light sources and components in display systems since the introduction of WLEDs in the 1960s [2]. The lighting industry is actively focusing on WLEDs, also regarded as the next generation of solid-state lighting (SSL) [3]. In recent years, WLEDs have gotten a lot of attention in comparison to traditional light sources like incandescent and fluorescent lamps because of their benefits like low energy consumption, higher rendering index (CRI), reliability, higher luminosity efficiency, longer lifetime, energy-saving qualities and environmental friendliness [4,5].

According to solid state lighting research, low cost and ease of preparation are essential criteria in phosphor synthesis. As a consequence, choosing the most excellent host from a plethora of options such as silicates, sulphates, phosphates, nitrates and vanadates is critical. Phosphors based on phosphate host matrices have become a major research area due to their wide variety of applications in lighting and displays. Phosphate based phosphors have a number of benefits, including a low cost, a high luminous efficiency, a low sintering temperature, a big band gap, greater thermal and chemical stability over a wide range of temperatures and a straightforward synthesis procedure. On a variety of phosphate based hosts, a number of phosphate based compounds with the generic formula $A^{I}{}_4{}^{IV}[XO_4]_3$

(where A is a metal ion with an oxidation state of +1 (I) to +4 (IV) and X = Cr, P, Si, Ge, S, Se, As, V, *etc.*) have been revealed. In the structure of eulytite type phosphate, the $A^{I\text{-}IV}$-site cations are randomly oriented, resulting in a disordered structure that is an excellent luminous material host [6].

Trivalent lanthanide ion-doped optical materials have drawn a lot of interest due to the abundance of emission colours based on 4*f*-4*f* or 5*d*-4*f* transitions [7]. Dy^{3+} is selected among the trivalent lanthanide ions in this research because it is most appropriate for the production of white light. Dy^{3+} ions typically exhibit two well-known emission bands: $^4F_{9/2} \rightarrow {}^6H_{15/2}$ in blue at (470–500 nm) and $^4F_{9/2} \rightarrow {}^6H_{13/2}$ in yellow at (570–600 nm). The luminescence properties of rare earth doped eulytite-type materials are quite good. According to previous study, eulytite type materials can serve as excellent matrices for solid lightning because of their disordered structure that promotes luminescence [8]. Several reports of eulytite type phosphates have been reported based on WLED application standards, including $NaCaBi_2(PO_4)_3:Dy^{3+},Eu^{3+}$ [9], $Sr_3Gd(PO_4)_3:Dy^{3+}$ [10], $Sr_3Bi(PO_4)_3:Dy^{3+}$ [11], $Ba_3Y(PO_4)_3:Dy^{3+}$ [12], $Sr_3Y(PO_4)_3:Dy^{3+}$ [13] and $MNa[PO_4]:Dy^{3+}$ [14]. The $NaBaBi_2[PO_4]_3$ combination is a potential host material for lanthanide ions doped phosphor. To the best of our knowledge, the photoluminescence properties of $NaBaBi_2[PO_4]_3:Dy^{3+}$ phosphors have yet to be determined.

In order to explore a white light phosphor for solid state lighting, a series of $NaBaBi_{(2-x)}(PO_4)_3:xDy^{3+}$ ($0.025 \le x \le 0.20$) phosphors were synthesized by high temperature solid state reaction in an air atmosphere. The structural and photoluminescence properties were explored, as well as the concentration quenching mechanism. The CIE chromaticity coordinates of the phosphors were calculated and discussed.

EXPERIMENTAL

Phosphor sample preparation: The $NaBaBi_{(2-x)}(PO_4)_3:xDy^{3+}$ phosphors were prepared by varying the dopant Dy^{3+} content *x* from 0.025 to 0.2 using a traditional high-temperature solid-state reaction method. Analytical grade Na_2CO_3, $BaCO_3$, Bi_2O_3, $NH_4H_2PO_4$ and Dy_2O_3 were procured from Sigma-Aldrich. Because high-purity raw ingredients were utilized, no purification was required. The raw ingredients were weighed and homogenized in an agate mortar for around 30 min according to the stoichiometric ratio. To ensure that all of the raw ingredients were thoroughly decomposed, the crushed phosphors were placed in a crucible and presintered at 400 ºC for 3 h inside the muffle furnace. After 30 min of pulverization, the powered phosphors were sintered for yet another 6 h at 800 ºC in the muffle furnace. The entire process has been carried out in an air atmosphere. Finally, the samples were allowed to cool to ambient temperature prior to being pulverized into powder for the measurements.

Characterization: The crystallinity and phase purity of the synthesized phosphors were investigated using a powder X-ray diffractometer (PXRD) with a Bragg-Brentano geometry and Cu*K*α radiation (λ = 1.5406 Å) at 40 kV and 40 mA. A Carl Zeiss Microscopy GmbH, field emission scanning electron microscope has been utilized to explore the surface morphology. A Fluoromax-4 Spectrofluorometer (Horiba Scientific) was used to determine the photoluminescence (PL) emission as well as the photoluminescence excitation (PLE) spectrum. Diffuse reflection spectra (DRS) were recorded using a UV-Vis-NIR spectrophotometer (V-670, Shimadzu) and white $BaSO_4$ powder was used as a reference standard. The chromaticity coordinate values were calculated using MATLAB software. All of these experiments were carried out at room temperature.

RESULTS AND DISCUSSION

XRD studies: To ensure phase formation and crystalline nature of the synthesized phosphors, XRD patterns of the as-prepared $NaBaBi_{(2-x)}(PO_4)_3:xDy^{3+}$ phosphor were obtained for various concentrations $x = 0$, 0.025, 0.05, 0.075, 0.1, 0.15 and 0.2 is shown in Fig. 1. The obtained phosphor samples could be significantly indexed to the appropriate standard phases of $NaBaBi_2(PO_4)_3$ (JCPDS card no. 47-0843), implying that they are single phase. There was no additional impurity phase found, indicating that Dy^{3+} ions doping had no effect on the host structure and demonstrating that the produced samples are of excellent phase purity. According to JCPDS card, the compound $NaBaBi_2(PO_4)_3$ has an eulytite type structure and a cubic crystal system with space group $I\bar{4}3d$ (220), lattice parameters $a = b = c = 10.2601$ Å, $a = b = c = 90°$, Z = 4 and cell volume = 1080.1 Å^3. Furthermore, Dy^{3+} occupied sites may be stated using eqn. 1 [15]:

$$D_r\ (\%) = \left(\frac{(R_s(CN) - R_d(CN))}{R_s(CN)} \right) \times 100 \qquad (1)$$

Here, D_r, CN, R_s and R_d are the radius percentage difference, coordination number and ionic radii of the host cation and doped ion, respectively. The radius percentage of difference (D_r) between the potential substitution ion Bi^{3+} (r = 1.03 Å) and the dopant ions Dy^{3+} (r = 0.912 Å) is determined to be 11.4% (for hexa-coordination), suggesting that dopant ions Dy^{3+} are occupying Bi^{3+} sites in the host lattice ($D_r < 30$) [16]. The substitution of Bi^{3+} ions by Dy^{3+} ions seemed to have no influ-ence on the charge balance of host lattice because the valence states of Dy^{3+} ions were compatible with those of Bi^{3+} ions. The average crystallite size of the samples was estimated using the Scherrer's equation to better understand their crystalline nature (eqn. 2):

$$D = \frac{k\lambda}{\beta \cos\theta} \qquad (2)$$

where, D is the average crystallite size, k is the dimensionless shape factor with a value of 0.9, λ is the X-ray wavelength (λ = 0.15406 nm), β is the line broadening full-width at half-maximum (FWHM in radians) and θ is the Bragg's diffraction angle in degrees [17]. For the optimal concentration of Dy^{3+} doped phosphor ($x = 0.075$), the crystallite size is found to be D = 59.3 nm.

Surface morphology: The surface morphology of optimum concentration of as-prepared $NaBaBi_{1.925}(PO_4)_3:0.075Dy^{3+}$ phosphor were investigated using field emission scanning electron microscopy (FESEM). Fig. 2 clearly revealed that the synthesized phosphors are in the nano-scale range of particles with irregular morphologies, which may be due to thermal decom-

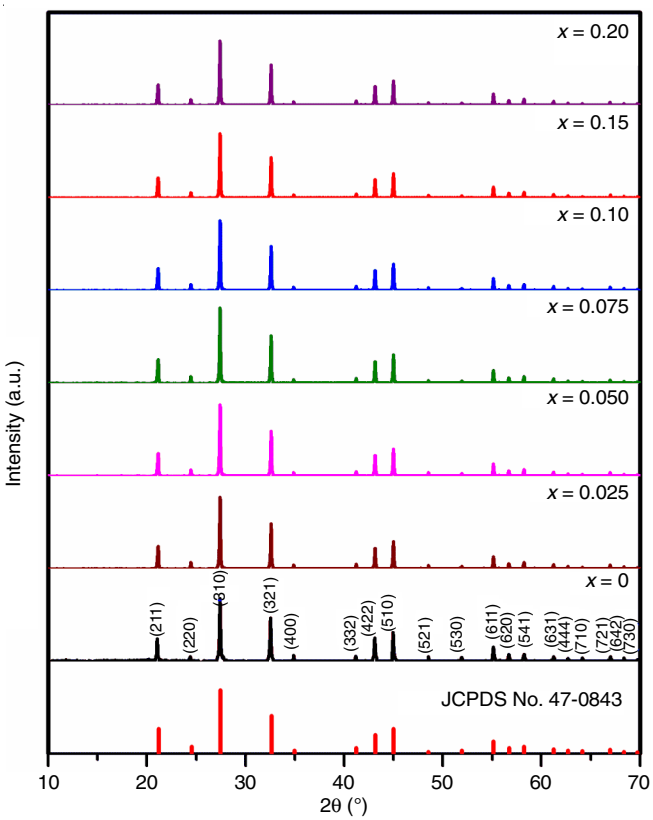

Fig. 1. XRD patterns of $NaBaBi_{(2-x)}(PO_4)_3$:xDy^{3+} for various concentrations (x = 0, 0.025, 0.05, 0.075, 0.1, 0.15 and 0.2)

position at elevated temperatures. It is made up of agglomerated particles and has a granular polycrystalline shape, as per FESEM images at different magnifications. They are certainly useful in a wide range of scientific and solid-state lighting device manufacturing applications [18].

UV-DRS studies: The optical absorption of host lattice, $NaBaBi_2(PO_4)_3$ and the Dy^{3+} doped phosphors were investigated using UV-visible diffuse reflectance spectroscopy in the 200-800 nm range. The DRS spectra of undoped host lattice $NaBaBi_2(PO_4)_3$ are shown in Fig. 3a and the band gap energy of the host matrix is shown in the inset. Between 400 and 800 nm, it has a high reflection status, then drops significantly between 350 and 200 nm, which corresponds to the band transition in the $NaBaBi_2(PO_4)_3$ host lattice.

The DRS spectra of $NaBaBi_{(2-x)}(PO_4)_3$:xDy^{3+} for x = 0.025, 0.05, 0.075, 0.1, 0.15 and 0.2 are shown in Fig. 3b. From 450 to 800 nm, a high percentage of reflectance is observed. A substantial absorption band in the wavelength range of 340 to 500 nm is found when Dy^{3+} ions are integrated into the host matrix. The photoluminescence excitation spectra in Fig. 4a matched very well with the absorption in $NaBaBi_2(PO_4)_3$:Dy^{3+} phosphor at 389 and 428 nm closely. The spin and parity forbidden transitions were responsible for low intensity of absorption lines (corresponding to the 4*f*-4*f* transition of Dy^{3+}) [19]. The band gap energies (E_g) of $NaBaBi_{(2-x)}(PO_4)_3$:xDy^{3+} phosphor were calculated using $(\alpha h\nu)^{1/n}$ *versus* wavelength traces. The nature and value of the optical band gaps may be

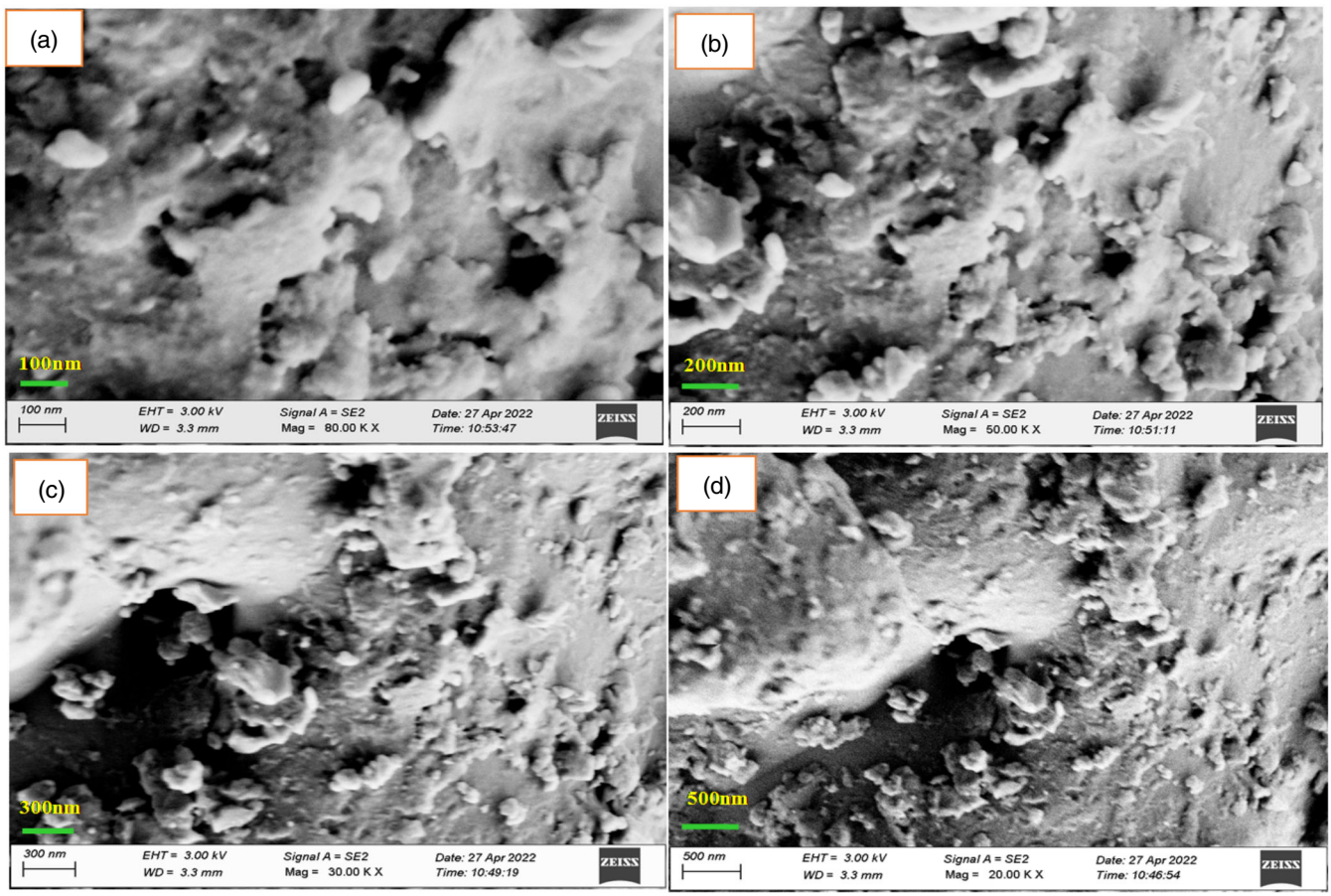

Fig. 2. FESEM images of $NaBaBi_{(2-x)}(PO_4)_3$:xDy^{3+} phosphor under different magnifications, 80, 50, 30 and 20 KX

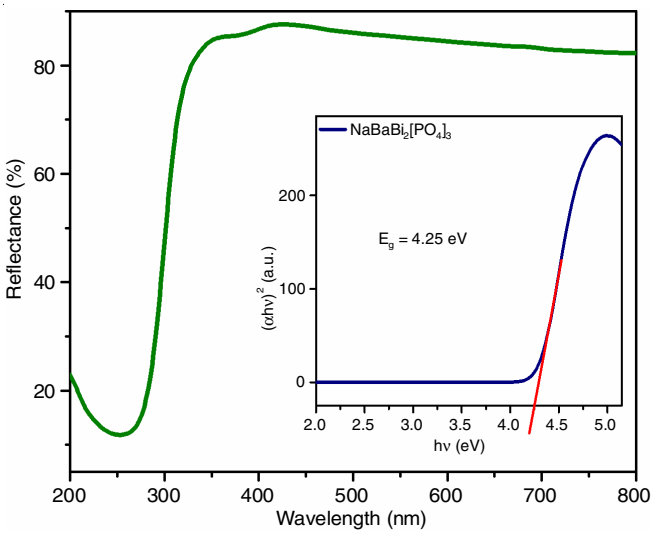

Fig. 3a. DRS of host $NaBaBi_2(PO_4)_3$ phosphor and the inset is band gap energy for the host lattice

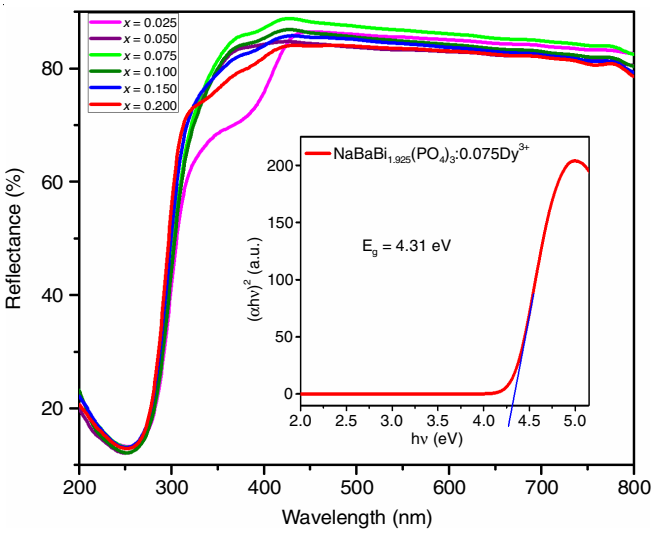

Fig. 3b. DRS of $NaBaBi_{(2-x)}(PO_4)_3$:xDy^{3+} (x = 0.025, 0.05, 0.075, 0.1, 0.15 and 0.2) phosphors and the inset shows the energy band gap for the optimum concentration x = 0.075

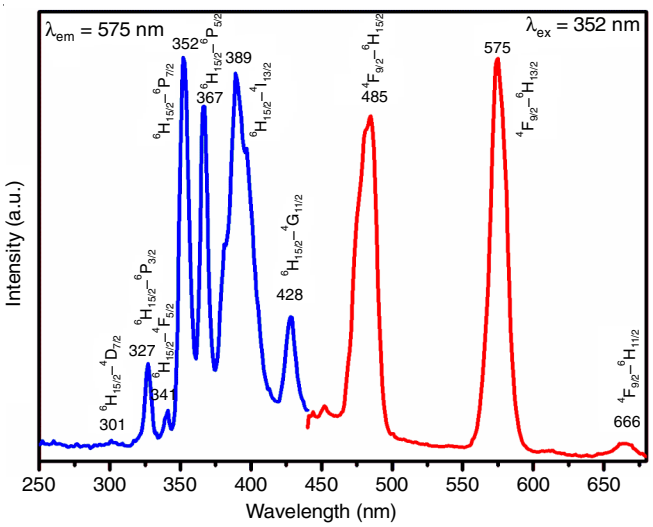

Fig. 4a. Photoluminescence excitation and emission spectra of $NaBaBi_{1.925}(PO_4)_3$:$0.075Dy^{3+}$ (monitored at λ_{ex} = 352 nm and λ_{em} = 575 nm)

evaluated utilizing fundamental absorption, which corresponds to electron excitation from the valence band to the conduction band. Eqn. 3 is the relationship between the absorption coefficient (α) and incident photon energy (hν):

$$(\alpha h\nu)^{1/n} = A(h\nu - E_g) \quad (3)$$

where A is a proportional constant, h is the Planck's constant, ν is the frequency of light, E_g is the material's band gap energy and n is an exponent depending on what kind of transition. The values of n = 1/2, 2 and 3/2 for direct allowed, indirect allowed and direct forbidden transitions, respectively. The $(\alpha h\nu)^{1/n}$ *versus* hν were plotted to determine the probable transitions and the associated band gaps were calculated by extrapolating the steepest portion of the graph on the h axis at $(\alpha h\nu)^{1/n}$ = 0. The host has an energy band gap of 4.25 eV, whereas the Dy^{3+} doped phosphor has an energy band gap of 4.27, 4.29, 4.31, 4.30, 4.33 and 4.35 eV for the concentrations x = 0.025, 0.05, 0.075, 0.1, 0.15 and 0.2. The modest change in E_g value can be attributed to the disorder generated in the host lattice as a consequence of lanthanide ion inclusion [20].

Photoluminescence properties: To explore the photoluminescence properties of the trivalent rare earth ion Dy^{3+} in $NaBaBi_2(PO_4)_3$ host, the excitation (PLE) and emission (PL) spectra were measured and depicted in Fig. 4a. The excitation spectrum of $NaBaBi_{1.925}[PO_4]_3$:$_{0.075}Dy^{3+}$ of phosphor by monitoring the emission wavelength at 575 nm is shown in Fig. 4a. This phosphor exhibits a series of intraconfigurational (4*f*-4*f* transitions) excitation peaks at 301, 327, 341, 352, 367, 389 and 428 nm corresponding to the electronic transitions from the ground state to excited state $^6H_{15/2} \rightarrow {}^4D_{7/2}$, $^6H_{15/2} \rightarrow {}^6P_{3/2}$, $^6H_{15/2} \rightarrow {}^4F_{5/2}$, $^6H_{15/2} \rightarrow {}^6P_{7/2}$, $^6H_{15/2} \rightarrow {}^6P_{5/2}$, $^6H_{15/2} \rightarrow {}^4I_{13/2}$ and $^6H_{15/2} \rightarrow {}^4G_{11/2}$, respectively [21,22]. The prominent excitation peaks in the excitation spectrum suggest that this phosphor is well suited for creating WLEDs utilizing near-UV or blue LED chips.

The emission spectrum reveals that the phosphor emits two strong emission peaks at 485 nm ($^4F_{9/2} \rightarrow {}^6H_{15/2}$) and 575 nm ($^4F_{9/2} \rightarrow {}^6H_{13/2}$), as well as one weak peak at 666 nm ($^4F_{9/2} \rightarrow {}^6H_{11/2}$), when excited at the most intense 352 nm ($^6H_{15/2} \rightarrow {}^6P_{7/2}$) excitation band. This emission band is composed of blue (485 nm), yellow (575 m) and red (666 nm). It is obvious that yellow emission band is relatively greater than blue emission band. The hypersensitive electric dipole transition, $^4F_{9/2} \rightarrow {}^6H_{13/2}$, is greatly impacted by the surrounding environment, but the magnetic dipole $^4F_{9/2} \rightarrow {}^6H_{15/2}$ transition is unaffected by the crystal field symmetry around the Dy^{3+} ion [23]. Because of its dominant hypersensitive electric dipole (ED) transition, $^4F_{9/2} \rightarrow {}^6H_{13/2}$ of Dy^{3+} ions are predicted to inhabit a low-symmetry site with no inversion center, in the host lattice [24].

Fig. 4b illustrates the relationship between emission intensity and variation in the Dy^{3+} doping concentration. It can be recognized that the emission intensity increases with Dy^{3+} doping concentration, peaking at x = 0.075, after which the emission intensity decreases, indicating that the critical concentration has been realized. The concentration quenching of luminescence is caused by energy transfer from one activator to another until all energy is exhausted. As a consequence,

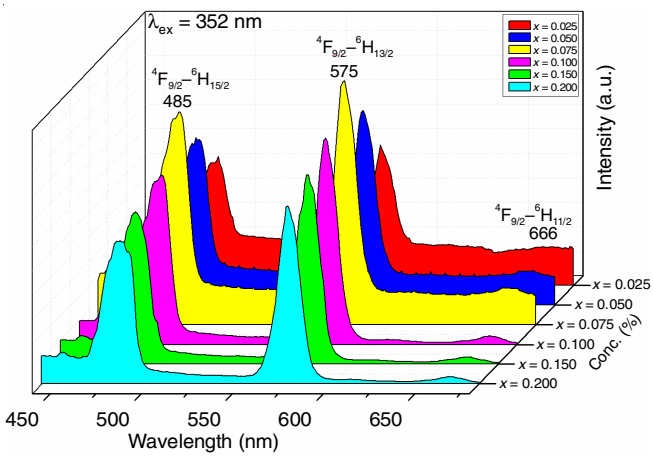

Fig 4b. Emission spectra of $NaBaBi_{(2-x)}(PO_4)_3:xDy^{3+}$ phosphors with different concentrations of Dy^{3+} ions under 352 nm excitation

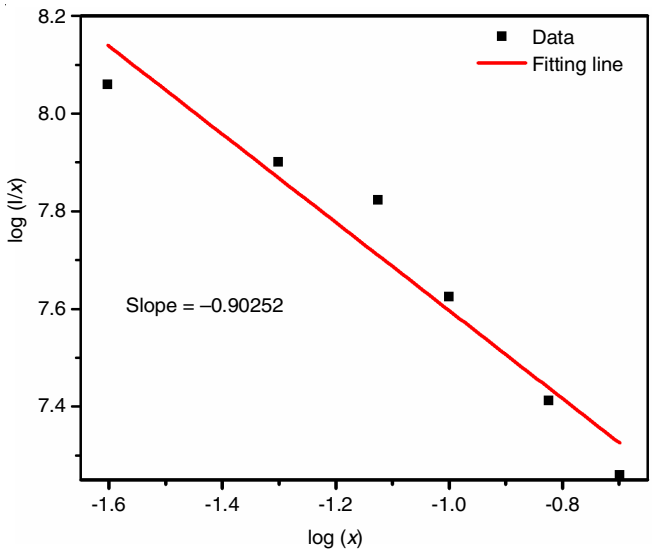

Fig. 4c. Curve of log (I/*x*) *vs.* log *x* in $NaBaBi_{(2-x)}(PO_4)_3:xDy^{3+}$ phosphor (λ_{ex} = 452 nm)

calculating the critical distance is essential (R_c) [22]. The Blasse formula [25] can be used to compute the critical radius distance (R_c) between activators ($RE^{3+} - RE^{3+}$) is given in eqn. 4:

$$R_c = 2\left(\frac{3V}{4\pi x_c N}\right)^{1/3} \quad (4)$$

where x_c is the critical concentration of the activator ion, N is the number of available sites for the activator ions in the unit cell and V is the volume of the unit cell. The critical transfer distance of xDy^{3+} centred in $NaBaBi_{(2-x)}(PO_4)_3$ phosphor is determined to be R_c = 19.01 Å using the optimal parameters of V, N and x_c (1080.1 Å, 4 and 0.075, respectively) [26].

If the Dy^{3+}–Dy^{3+} distance is greater than 5 Å, the exchange interaction is ineffectual and only the multipolar interaction is relevant; if the Dy^{3+}–Dy^{3+} distance is less than 5 Å, then the exchange interaction is effective [27]. The multipolar interaction is the predominant method of concentration quenching, as evidenced from the R_c value of Dy^{3+}–Dy^{3+} for $NaBaBi_2(PO_4)_3$:Dy^{3+} phosphor.

The microscopic method of interaction between luminous centres defines the energy transfer type. Van Uitert [28] created a theoretical background for the correlation between luminous intensity and doping concentration in his early research. There are three energy-transfer manifestations of multipolar interaction, according to Van Uitert's report: dipole–dipole (d–d), dipole–quadrupole (d–q) and quadrupole–quadrupole (q–q) interactions. The change in emission intensity from the multipolar interaction emitting level may also be used to quantify the intensity of multi-polar interaction level [28]. Dexter's theory may also be utilized to analyse the type of interaction between the activators using eqn. 5:

$$\frac{I}{x} = K[1+\beta(x)^{Q/3}]^{-1} \quad (5)$$

there, I denotes for the emission spectrum's integral intensity, *x* for the activator concentration, I/*x* for the emission intensity per activator concentration, K and β are constants for a given host in the identical excitation condition.

Q denotes the sort of interaction between rare earth ions, with Q = 3 indicating energy transfer among the closest neighbours and Q = 6, 8, 10 indicating d–d, d–q and q–q interactions, respectively. As a result, further calculations are defined which sort of interaction contributes to the energy transfer. Eqn. 5 can be effectively simplified to eqn. 6 for $\beta(x)^{Q/3} \approx 1$ as follows:

$$\log\left(\frac{I}{x}\right) = A - \frac{Q}{3}\log x \quad (6)$$

where, A = log k – log β.

The linear fitting of the log (x) and log (I/x) value resulted in slope value is -0.90252 for blue and yellow emission, respectively. For linear fitting, the Q value estimated using eqn. 5 is 2.70, which is close to 3, which suggested that the concentration quenching must be caused by energy transfer among the closest-neighbor ions in $NaBaBi_{(2-x)}(PO_4)_3:xDy^{3+}$ phosphors [29].

CIE chromaticity coordinates: The chromaticity diagram from the Commission International de l'Eclairage (CIE) demonstrates the importance of coordinates in determining a phosphor's exact emission colour and colour purity. The emission spectra (monitored at λ_{ex} = 452 nm) at the optimal concentration *x* = 0.075 were used to compute the CIE chromaticity coordinates of phosphors. The colour coordinates of $NaBaBi_{1.925}(PO_4)_3$: $0.075Dy^{3+}$ for full emissions were estimated to be *x* = 0.341 and *y* = 0.374. As seen in Fig. 5, the coordinates were close to "ideal white" (0.333, 0.333), indicating a cool white colour tone.

Conclusion

In summary, a series of white emitting phosphors, $NaBaBi_{(2-x)}Dy_x(PO_4)_3$, are achieved by a high-temperature solid state reaction. The XRD results confirmed that the host matrix belongs to the eulytite type structure and crystallized in the cubic phase of space group $I\bar{4}3d$. The FESEM images revealed the nanocrystalline nature of the prepared phosphors. The band gap between the host and Dy^{3+} doped phosphors was estimated to be between 4.25 and 4.35 eV. The photoluminescence result inferred that the phosphors display the efficient excitations in

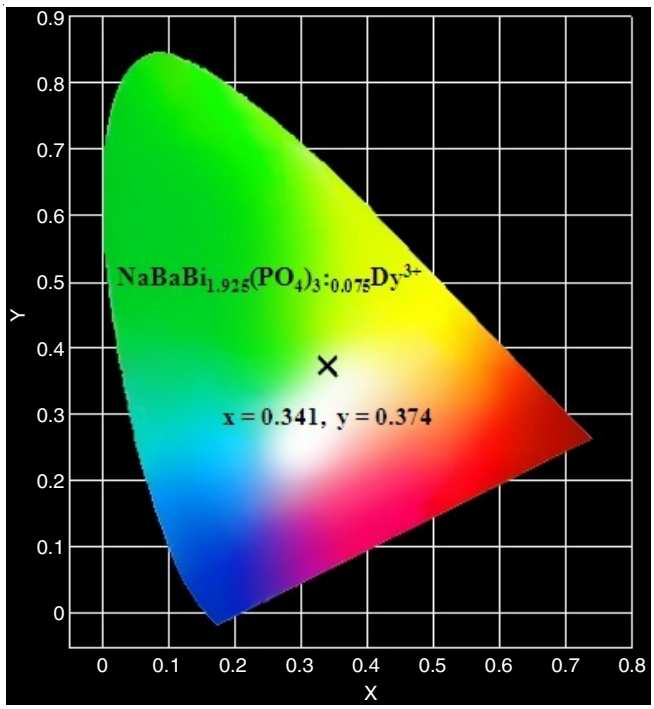

Fig. 5. CIE chromaticity diagram for $NaBaBi_{1.925}(PO_4)_3$:0.075Dy^{3+} sample under 405 nm

near UV and blue regions, originating from the 4*f*-4*f* transitions of Dy^{3+}. This means that the phosphor can be effectively excited by UV chips for potential applications in WLEDs. The emission spectra showed two dominant emission bands in the blue ($^4F_{9/2} \rightarrow {}^6H_{15/2}$) and yellow ($^4F_{9/2} \rightarrow {}^6H_{13/2}$) regions. The yellow emission is stronger than the blue emission as the Dy^{3+} ions are in a low-symmetry site. The optimum dopant concentration of Dy^{3+} ions is $x = 0.075$. Energy transfer between nearest-neighbour ions is the base of the concentration quenching mechanism. The CIE chromaticity coordinates values lie in the ideal white region. All of these characteristics indicated that Dy^{3+} doped $NaBaBi_2(PO_4)_3$ phosphors have substantial potential for usage in near-UV or blue light-excited WLED applications.

CONFLICT OF INTEREST

The authors declare that there is no conflict of interests regarding the publication of this article.

REFERENCES

1. M. Shang, C. Li and J. Lin, *Chem. Soc. Rev.*, **43**, 1372 (2014); https://doi.org/10.1039/C3CS60314H
2. J. Hye Oh, S. Ji Yang and Y. Rag Do, *Light Sci. Appl.*, **3**, 141 (2014); https://doi.org/10.1038/lsa.2014.22
3. C.F. Guo, W. Zhang, L. Luan, T. Chen, H. Cheng and D. Huang, *Sens. Actuators B Chem.*, **133**, 33 (2008); https://doi.org/10.1016/j.snb.2008.01.065
4. H. Shanshan and T. Wanjun, *J. Mater. Sci.*, **48**, 5840 (2013); https://doi.org/10.1007/s10853-013-7379-5
5. E.F. Schubert and J.K. Kim, *Science*, **308**, 1274 (2005); https://doi.org/10.1126/science.1108712
6. V.I. Pet'kov, A.S. Dmitrienko and A.I. Bokov, *J. Therm. Anal. Calorim.*, **133**, 199 (2018); https://doi.org/10.1007/s10973-017-6676-7
7. M.M. Shang, D.L. Geng, D.M. Yang, X.J. Kang, Y. Zhang and J. Lin, *Inorg. Chem.*, **52**, 3102 (2013); https://doi.org/10.1021/ic3025759
8. N. Guo, W. Lü, Y. Jia, W. Lv, Q. Zhao and H. You, *ChemPhysChem*, **14**, 192 (2013); https://doi.org/10.1002/cphc.201200836
9. E.A. Rathnakumari, M. Jayachandiran and S.M.M. Kennedy, *Optik*, **186**, 221 (2019); https://doi.org/10.1016/j.ijleo.2019.04.048
10. Q. Xu, J. Sun, D. Cui, Q. Di and J. Zeng, *J. Lumin.*, **158**, 301 (2015); https://doi.org/10.1016/j.jlumin.2014.10.034
11. Z. Yang, Y. Liu, C. Liu, F. Yang, Q. Yu, X. Li and F. Lu, *Ceram. Int.*, **39**, 7279 (2013); https://doi.org/10.1016/j.ceramint.2013.02.044
12. Q. Liu, Y. Liu, Y. Ding, Z. Peng, X. Tian, Q. Yu and G. Dong, *Ceram. Int.*, **40**, 10125 (2014); https://doi.org/10.1016/j.ceramint.2014.01.137
13. Y.W. Seo, S.H. Park, S.H. Chang, J.H. Jeong, K.H. Kim and J.S. Bae, *Ceram. Int.*, **43**, S0272 (2017); https://doi.org/10.1016/j.ceramint.2017.03.205
14. A. Balakrishna and O.M. Ntwaeaborwa, *Actuators B Chem.*, **242**, 305 (2017); https://doi.org/10.1016/j.snb.2016.11.060
15. K. Li, H. Lian, M. Shang and J. Lin, *Dalton Trans.*, **44**, 20542 (2015); https://doi.org/10.1039/C5DT03565A
16. R.D. Shannon, *Acta Crystallogr. A*, **32**, 751 (1976); https://doi.org/10.1107/S0567739476001551
17. T. Yaba, R. Wangkhem and N.S. Singh, *J. Alloys Compd.*, **843**, 156022 (2020); https://doi.org/10.1016/j.jallcom.2020.156022
18. M.M. Yawalkar, G.D. Zade, K.V. Dabre and S.J. Dhoble, *Luminescence*, **31**, 1037 (2016); https://doi.org/10.1002/bio.3006
19. Y. Deng, S. Yi, J. Huang, J. Xian and W. Zhao, *Mater. Res. Bull.*, **57**, 85 (2014); https://doi.org/10.1016/j.materresbull.2014.05.035
20. R. Borja-Urby, L.A. Diaz-Torres, P. Salas, M. Vega-Gonzalez and C. Angeles-Chavez, *Mater. Sci. Eng. B*, **174**, 169 (2010); https://doi.org/10.1016/j.mseb.2010.04.024
21. X. Li, L. Guan, M. Sun, H. Liu, Z. Yang, Q. Guo and G. Fu, *J. Lumin.*, **131**, 1022 (2011); https://doi.org/10.1016/j.jlumin.2011.01.015
22. P. You, G. Yin, X. Chen, B. Yue, Z. Huang, X. Liao and Y. Yao, *Opt. Mater.*, **33**, 1808 (2011); https://doi.org/10.1016/j.optmat.2011.06.018
23. G. Seeta Rama Raju, H.C. Jung, J.Y. Park, C.M. Kanamadi, B.K. Moon, J.H. Jeong, S.-M. Son and J.H. Kim, *J. Alloys Compd.*, **481**, 730 (2009); https://doi.org/10.1016/j.jallcom.2009.03.095
24. Y. Cao, Y. Liu, H. Feng and Y. Yang, *Ceram. Int.*, **40**, 15319 (2014); https://doi.org/10.1016/j.ceramint.2014.06.127
25. G. Blasse, *Phys. Lett. A*, **28**, 444 (1968); https://doi.org/10.1016/0375-9601(68)90486-6
26. J. Du, D. Xu, X. Gao, J. Li, Z. Yang, X. Li and J. Sun, *J. Mater. Sci.: Mater. Electron.*, **29**, 573 (2018); https://doi.org/10.1007/s10854-017-7949-4
27. G. Blasse and B.C. Grabmarier, Luminescent Materials, Springer-Verlag, Berlin, p. 99 (1994).
28. L.G. Van Uitert, *J. Electrochem. Soc.*, **114**, 1048 (1967); https://doi.org/10.1149/1.2424184
29. M. Yu, W. Zhang, G. Yan, S. Dai, Z. Qiu and L. Zhang, *Ceram. Int.*, **44**, 2563 (2018); https://doi.org/10.1016/j.ceramint.2017.11.012